

d^2 , d^3 , and d^4 M_3C_2 Transition Metal Carbides (MXenes) as Catalysts for CO_2 Conversion into Hydrocarbon Fuels: A Mechanistic and Predictive DFT Study

Neng Li,^{a, ‡} Luis Miguel Azofra,^{b, ‡} Xingzhu Chen,^a Douglas R. MacFarlane,^b Xiujuan Zhao,^a and Chenghua Sun^{b, *}

^aState Key Laboratory of Silicate Materials for Architectures, Wuhan University of Technology, Hubei, 430070, China

^bARC Centre of Excellence for Electromaterials Science (ACES), School of Chemistry, Faculty of Science, Monash University, Clayton, VIC 3800, Australia

KEYWORDS: CO_2 conversion; CO_2 capture; MXenes; reaction mechanisms; DFT+U; DFT-D3

ABSTRACT: The functioning of 2D d^2 , d^3 , and d^4 transition metal carbides (MXenes) with formulae $M_{n+1}C_n$ ($n = 2$) as CO_2 conversion catalysts has been proved by well-resolved density functional theory (DFT) and DFT+U theoretical calculations. Whilst MXenes from the d^2 series ($M = Ti, Zr, \text{ and } Hf$) have demonstrated active behaviors for the capture of CO_2 , the V_3C_2 , Nb_3C_2 , Cr_3C_2 , and Mo_3C_2 materials exhibit the most promising results for their application in the selective CO_2 conversion into CH_4 , with limiting reaction energies of 1.55, 1.75, 0.69, and 1.24 eV, respectively, at DFT+U computational level plus explicit DFT-D3 dispersion corrections, and specially highlighting the role of Cr_3C_2 due to its theoretically predicted low over-potential. Moreover, important features have been predicted during the first hydrogenation step towards the formation of the $OCHO\cdot$ and $HOCO\cdot$ radical species, exhibiting spontaneous reaction energies in the $OCHO\cdot$ obtaining for such promising carbides from the d^3 and d^4 groups. Our results provide novel insights in the computer-aided searching of high performance catalysts and the understanding of reaction mechanisms for CO_2 . Finally, it is hypothesized that the capture of CO_2 along the early step of the reaction is spontaneously produced without pass from a physisorbed state, being the strength of such capture larger than the computed binding energies for the chemisorption of H_2O , offering encouraging perspectives for the experimental testing of our materials in water environment.

INTRODUCTION

The massive and large-scale anthropogenic carbon dioxide (CO_2) emissions into the atmosphere, as a consequence of our heavy reliance on imported non-renewable energy sources,¹ have triggered the intensification of the greenhouse effect, a serious environmental problem which has been related to climate change.² The magnitude of this issue confronts us with an unprecedented challenge: significant reductions in CO_2 emissions and the search for realistic alternatives to the energy sources based on petrol are critical.

In this regard, CO_2 conversion technology,³ as an energy storage alternative due to its relevance for the environment and sustainability, has been actively developed towards the production of hydrocarbon ‘green fuels’ that can be re-burned for energy generation with a zero-balance of greenhouse emissions. Since the CO_2 conversion technology is profiled as one of the several solutions to the so-called ‘ CO_2 problem’, a vast and rich literature has emerged in such topic in the recent years: a diverse selection of materials have been extensively used and optimized such as titania-based (TiO_2) semiconductors,⁴⁻⁶ Cu and photo-catalytic active Cu_2O ,⁷⁻⁹ 2D

metal-free meshes as functionalized graphene oxide¹⁰ or graphite-like carbon nitride ($g-C_3N_4$),¹¹ among others.¹²⁻¹⁵ However and as indicated by Whipple *et al.*,¹⁶ many advances in the field are still needed to address the energy efficiency and the reaction rate issues, among others limitations.

From a mechanistic point of view, the CO_2 conversion process through electrochemical approaches consists in successive electro-reductions by inclusion of a set of H^+/e^- pairs, and depending on the total even number of H^+/e^- couples transferred along the whole reaction (from two to eight), different hydrocarbon compounds such as carbon monoxide (CO) or formic acid (HCOOH), formaldehyde (H_2CO), methanol (CH_3OH), or methane (CH_4), can be obtained.¹⁷ In this regard, an advanced understanding of the reaction mechanism is essential for the design of novel catalysts, specially when specific products are targeted. On the one hand, catalysis cannot occur if there is no effective physicochemical contact between gas molecules and the catalyst surface. A non-covalent interaction, normally of $O=C=O_{lp} \cdots Y$ nature with “Y” being an electro-positive atom, is required in order to adsorb CO_2 on the surface. However, CO_2 fixa-

tion is often thermodynamically non-spontaneous under mild conditions (i.e. ambient temperatures and pressures) and additional energy/pressure is required to enhance such contact. Once it is adsorbed, the next challenge is the first hydrogenation step, denoted by the single-electron $\text{CO}_2 + \text{e}^- \rightarrow \text{CO}_2^{\bullet-}$ process. This represents a large impediment for the overall process since a significant amount of energy is required. In that regard, a strongly negative reduction potential of -1.90 V vs. NHE is exhibited,¹⁸ constituting the limiting step of the whole electrochemical reaction even when catalysts come into play. In addition to that, reduction potentials vs. NHE at neutral pH indicate a very poor selectivity for the isolated transformations into the aforementioned potential hydrocarbon products. To overcome these issues, the finding of novel strategies, specially new catalysts, is required.

Recent work carried out in our group have provided novel insights along the early stages of the CO_2 conversion mechanism when doping two dimensional (2D) boron nitride nano-sheets or meshes (BNs) with beryllium.¹⁹ As the consequence of the insertion of such electron-deficient atoms to the 2D network, important diminutions in the reaction energies were demonstrated for the CO_2 fixation and the first hydrogenation steps, i.e. due to the very deep π -hole generated on the Be-doped surface environment, the CO_2 adsorption became spontaneous in terms of the Gibbs free binding energy. More remarkably, the radical HOCO^\bullet and OCHO^\bullet species formed as result of the first H^+/e^- gain also exhibited spontaneous thermodynamics, with Gibbs free reaction energies at room temperature being equal to -0.45 and -0.98 eV, respectively. For classical semiconductors, the first proton-electron transfer often constitutes the limiting step of the whole reaction,^{18, 20, 21} while the outcomes generated through our DFT results indicate that this can be effectively changed through introducing special active sites on the surface.

However, despite the significance of such insights and the theoretical value from the computer-aided design of catalysts perspective, the difficulties involving Be-doping of BNs, as well as the high toxicity of beryllium,²² limit its potential applicability. In this context and following similar features and mechanisms, transition metal carbides emerge as promising candidates for such purposes. Recent investigations carried out by Naguib *et al.*²³ have demonstrated that the exfoliation of strong primary bond containing solids, such as MAX phase powders of Ti_3AlC_2 into Ti_3C_2 , labeling this novel kind of 2D materials as ‘MXenes’ due to their similarity with graphene. As has been recently summarized by Gogotsi and co-workers,²⁴ the etching out of the ‘‘A’’ layers from MAX phases with formulae $\text{M}_{n+1}\text{AX}_n$, which ‘‘M’’ an early transition metal, ‘‘A’’ an atom from the triel or tetrel groups (i.e. icosagens and crystallogens, respectively), and ‘‘X’’ = C or N with $n = 1, 2,$ and 3 , produces the synthesis of their respective MXenes with formulae

M_{n+1}X_n prior applying sonication technique. In this regard, not only Ti_3C_2 has been synthesized *via* this procedure, but also Ti_2C , Nb_2C , V_2C , $(\text{Ti}_{0.5}\text{Nb}_{0.5})_2\text{C}$, $(\text{V}_{0.5}\text{Cr}_{0.5})_2\text{C}$, $(\text{Nb}_{0.8}\text{Ti}_{0.2})_4\text{C}_3$, $(\text{Nb}_{0.8}\text{Zr}_{0.2})_4\text{C}_3$, Ti_3CN , Ta_4C_3 , Mo_2TiC_2 , $\text{Mo}_2\text{Ti}_2\text{C}_3$, or Cr_2TiC_2 , among others,^{23, 25, 26-28} which with large specific surface area are typically needed to obtain large capacitances for further CO_2 capture applications.

MXenes, such 2D solids,²⁴ have generated recent interest because of their outstanding electronic properties which can be exploited for innumerable industrial and biomedical applications. Multilayer MXenes are conductively similar to multilayer graphene. However, unlike graphene, MXenes can be easily dispersed in aqueous solutions because of their hydrophilic properties. Also, the inherent metallic character of MXenes may be modified to act as semiconductor once the surface is $-\text{F}$ or $-\text{OH}$ terminated.²⁵

In term of real applications, MXenes have already been demonstrated to be promising candidates for energy storage applications such as Li-ion batteries,²⁹⁻³¹ non-Li-ion batteries,³² electrochemical supercapacitors,³³⁻³⁵ and fuel cells.³⁶ Apart from the energy storage applications, MXenes were tested as photocatalytic materials,³⁷ gas sensors,³⁸ biosensors,³⁹ and transparent, conductive electrodes.⁴⁰

In the recent years, some literature has emerged describing the applicability of metal carbides as catalytic substrate for hydroprocessing, water splitting technology,⁴¹⁻⁴⁴ given the inherent properties of these materials with high specific areas and cleanness surfaces,⁴⁵ good electrical conductivities, stability, and hydrophilic behaviors.²⁵ Based on this background, we hypothesize and report theoretical evidences highlighting the function of d^2 , d^3 , and d^4 MXenes, transition metal carbides with formulae M_{n+1}C_n ($n = 2$) as CO_2 capture and conversion catalysts. In this regard, our DFT and state-of-the-art DFT+ U studies plus dispersion corrections predict active behaviors for the capture of CO_2 , being the strength of such capture larger than the computed binding energies for the chemisorption of H_2O . These inherent features expect an active physics for the CO_2 conversion mechanism: while injection of CO_2 solute is spontaneously produced on the material, the hydrophilic and high electrical conductivity advert the effective electro-reductions in both the H^+ attachments and electrons providing.

COMPUTATIONAL DETAILS

The mechanism for the electrochemical conversion of CO_2 into hydrocarbon compounds catalyzed by d^2 (Ti, Zr, and Hf), d^3 (V, Nb, and Ta), and d^4 (Cr and Mo) 2D transition metal carbides or MXenes, with formulae M_{n+1}C_n ($n = 2$), has been studied by means of density functional theory (DFT) through the generalized gradient approximation (GGA) with the Perdew-Burke-

Ernzerhof (PBE) functional,⁴⁶ using a plane-wave cut-off energy of 400 eV.^{47, 48} Concerning the periodic boundary conditions, the Brillouin zone was sampled by $3 \times 3 \times 1$ k -points using the Monkhorst-Pack scheme, after the tests with a larger set of k -points to make sure that there was no significant changes in the calculated energies. In order to avoid interactions between periodic images, a vacuum distance of 20 Å was imposed between different layers. At first stage, full optimizations were carried out using energy and force convergence limits equal to 10^{-4} eV/atom and $|0.05|$ eV/Å, respectively. For energy calculations, van der Waals interactions were taken into account through the Grimme DFT-D2 method.⁴⁹ In order to evaluate the zero point energy (ZPE) as well as the thermal corrections terms, additional calculations over the Γ points were carried out.

After the first-round calculations based on gas-phase models, the d^3 V_3C_2 and Nb_3C_2 , and the d^4 Cr_3C_2 and Mo_3C_2 surfaces have identified as the most promising catalysts for the CO_2 conversion. To further examine such results, additional Hubbard-like parameters have been included through the DFT+ U approach in the form developed by Dudarev *et al.*,^{50, 51} to treat the strong on-site Coulomb interactions of the d -like localized electrons in M_3C_2 , which are not correctly described *via* classical GGA-based DFT. In our case, U terms equal to 3.1, 3.0, 3.5, and 3.5 eV have been employed for V, Nb, Cr, and Mo, respectively.⁵²⁻⁵⁵ Over such DFT+ U re-optimizations, explicit dispersion correction terms to the energy were employed through the use of the DFT-D3 method with the standard parameters programmed by Grimme and co-workers.^{56, 57} With the aim to obtain more accurate values, computational settings were modified using a plane-wave cut-off energy of 450 eV, $|0.02|$ eV/Å as force convergence limit, and the Brillouin zone was expanded by $5 \times 5 \times 1$ k -points. All optimization calculations have been performed through the facilities provided by the Vienna *Ab-Initio* Simulation Package (VASP, version 5.3.5).⁵⁸⁻⁶¹

Finally, Eqn. (1) has been applied to calculate the reaction energies, where n is the number of H^+/e^- pairs transferred, m the number of H_2O molecules released, and p the number of CH_4 molecules released, if applicable. In such context, Nørskov and co-workers²⁰ estimate that the chemical potential of the H^+/e^- pair has the half value of the chemical potential of the dihydrogen (H_2) molecule [see Eqn. (2)].

$$\Delta G_R = G(\text{surf} \cdot CO_{2-m-p} H_{n-2m-4p}) + m G(H_2O) + p G(CH_4) - G(\text{surf}) - G(CO_2) - n/2 G(H_2) \quad (1)$$

$$\mu(H^+/e^-) = 1/2 \mu(H_2) \quad (2)$$

RESULTS AND DISCUSSION

Transition metal carbides (MXenes) with formulae $M_{n+1}C_n$ ($n = 2$) and $M = Ti, Zr, Hf, V, Nb, Ta, Cr,$ and Mo (hereafter simply referred as M_3C_2), are strongly bonded graphene-similar 2D materials composed by five layers of atoms in which carbons are in the inner layers being six-fold coordinated (labeled as 6c-C in **Fig. 1**) with two kinds of transition metals: those constituting the central inner layer (also hexa-coordinated) and the three-fold terminated (labeled as 3c-M in **Fig. 1**) which are specially reactive due to their empty d -like orbitals, and therefore where the catalytic activity will take place.

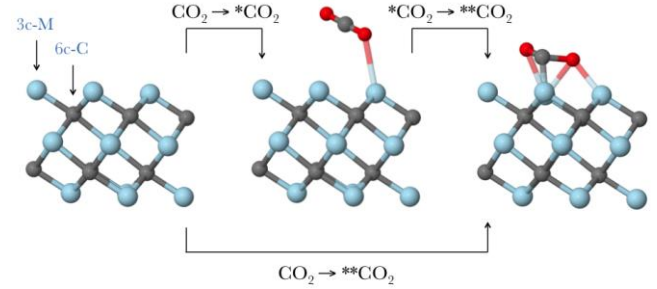


Figure 1. Proposed paths for the CO_2 interaction with the M_3C_2 MXenes surfaces: clean surface (left), CO_2 physisorption (center), and CO_2 chemisorption (right). 3c-M and 6c-C labels refer to three-fold transition metal and six-fold carbon atoms, respectively.

As indicated in **Fig. 1**, the interaction between CO_2 and the M-terminated surface of the MXenes might be carried out either through a physical fixation (physisorption) where CO_2 is attached to the surface through a non-covalent interaction of $O=C=O_{lp} \cdots M$ nature (**Fig. 1**, center), or through a chemisorbed process in which CO_2 is formally bound (**Fig. 1**, right). Gibbs free binding energies at room temperature (ΔG_b) display clear differences in respect to the thermodynamic stability in each case. On the one hand, **Table 1**, the CO_2 physisorption step is characterized by non-spontaneous binding energies, between 0.15 and 0.35 eV. This is in contrast to the case of Ta_3C_2 (see **Table 1**) as catalyst in which no minimum was located and Ti_3C_2 where the physical CO_2 fixation is spontaneously produced with -0.59 eV. On the other hand, the MXenes seem to be active towards CO_2 chemisorption, exhibiting spontaneous binding energies decreasing in strength as we move along the group, i.e. surfaces for d^2 MXenes are stronger capture materials than d^3 and d^3 stronger than d^4 . At this point, the question arising is: does the process of capture occur directly or is it done in two stages after passing the barrier imposed by the CO_2 physisorption?

In this regard, since MXenes are highly reactive surfaces, it seems contradictory to find such high barriers for the CO_2 fixation step, with values comparable or even larger than those observed with less-reactive surface materials, such as rutile $TiO_2(110)$.⁶² Comparing both classical DFT test results including van der Waals

Table 1. Gibbs Free Reaction Energies (in eV), calculated at PBE (GGA-DFT) computational Level (Thermal and ZPE Corrections included). All values are commonly referred to the Clean Surface and the Isolated Reactive Gases (0.00 eV). Note: * and ** Symbols Refer to Physisorbed and Chemisorbed Species, respectively.

	Ti ₃ C ₂	Zr ₃ C ₂	Hf ₃ C ₂	V ₃ C ₂	Nb ₃ C ₂	Ta ₃ C ₂	Cr ₃ C ₂	Mo ₃ C ₂
*CO ₂	-0.59	0.17	0.18	0.29	0.35	—	0.25	0.15
**CO ₂	-2.99	-3.16	-3.03	-1.45	-1.61	-2.29	-1.28	-2.12
**OCHO•	-2.05	-2.25	-2.88	-1.38	-1.72	-1.59	-1.60	-1.77
**HOCO•	-2.07	-2.49	-2.79	-1.40	-1.56	-1.94	-1.74	-1.94
**•OCH ₂ O•	-3.53	-4.09	-4.32	-1.93	-2.25	-2.88	-1.62	-1.69
**HCOOH	-1.02	-2.20	-2.48	-0.15	-0.15	-0.35	-0.01	-0.83
**CO	-1.27	-1.19	-1.61	-1.53	-1.49	-1.90	-2.09	-2.39
**HOCH ₂ O•	-2.50	-2.84	-3.13	-1.60	-1.92	-2.59	-1.88	-2.21
**HOCH ₂ OH	-1.14	-1.10	-1.55	-0.64	-0.73	-1.15	-0.73	-0.97
**H ₂ CO	-2.55	-3.31	-3.41	-1.91	-2.28	-2.50	-1.89	-2.00
*H ₂ CO	1.05	0.94	0.89	0.91	0.96	0.85	0.96	0.89
**CH ₂ OH•	-1.71	-2.17	-2.00	-1.37	-1.49	-2.07	-1.63	-1.79
**CH ₃ O•	-3.06	-3.23	-3.44	-2.31	-2.49	-3.11	-2.24	-2.68
**CH ₂	-2.01	-2.08	-1.38	-1.16	-1.69	-2.54	-1.86	-2.34
*CH ₃ OH	-0.08	-0.05	-0.12	0.21	-0.06	0.08	0.20	0.01
**CH ₃ •	-2.25	-2.58	-3.07	-2.46	-2.70	-3.49	-2.73	-3.23
*CH ₄	-1.41	-0.91	-1.15	-2.36	-1.00	-1.06	-0.78	-0.96
**O .. *CH ₄	-3.97	-4.30	-4.48	-2.59	-3.13	-3.44	-2.56	-2.64
**OH•	-4.09	-4.14	-4.29	-3.19	-3.41	-3.85	-3.23	-3.44
**H ₂ O	-2.54	-2.47	-2.54	-1.96	-1.89	-2.16	-2.07	-2.42

interactions through the Grimme’s DFT-D2 method and state-of-the-art and more accurate DFT+*U* calculations with explicit dispersion corrections *via* the DFT-D3 method (see **Tables 1** and **2**), it seems that as consequence of the force convergence settings (see **Computational details** section), physisorbed CO₂ minima appear as DFT artifacts, allowing us to conclude that CO₂ directly interacts with the surface through a spontaneous and exothermic process that produces its capture.

More remarkable are the huge differences shown between the Gibbs free binding energies computed at PBE/DFT-D2 and DFT+*U*/DFT-D3 levels of theory. In this regard, the strong on-site Coulomb interactions of the *d*-like localized electrons in M₃C₂ treated through the inclusion of explicit *U* Hubbard-like parameters, seems to be essential in the adequate description of the captured CO₂ steps: comparisons for ΔG_b in the *d*³ V₃C₂ and Nb₃C₂, and the *d*⁴ Cr₃C₂ and Mo₃C₂ materials differ in around 1.0-1.3 eV, supporting the spontaneity of the chemisorption process, but correcting the errors derived from over-estimated interactions between CO₂ and the M-terminated MXene surfaces.

The outcomes presented in this work are of great significance since they suggest that *d*²-*d*⁴ M₃C₂ MXenes are capable of spontaneously producing the capture of CO₂, overcoming the mechanistic limitation imposed by this first step of the CO₂ fixation, that as has been comment-

ed before, usually demands the input of energy/pressure to enhance the contact on the surface.⁶³

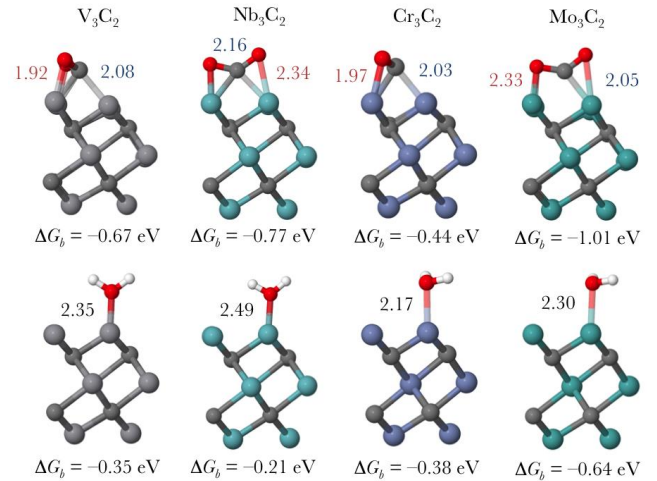


Figure 2. At top, captured CO₂ minima. Selected distances in dark blue and red indicate the proximal C–M and O–M distances, respectively, in Å. At bottom, H₂O chemisorption steps with proximal O–M distances in Å. Gibbs free binding energies at room temperature calculated at DFT+*U*/DFT-D3 computational level, with *U* = 3.1, 3.0, 3.5, and 3.5 eV for V, Nb, Cr, and Mo, in their respective M₃C₂ MXenes.

Table 2. Gibbs Free Reaction Energies (in eV), calculated at DFT+*U*/DFT-D3 (See **Computational Details**) Computational Level (Thermal and ZPE Corrections included) for d^3 V_3C_2 and Nb_3C_2 , and d^4 and Cr_3C_2 and Mo_3C_2 materials. All values are referred to the clean surface and the isolated reactive gases (0.00 eV). Note: * and ** Symbols Refer to Physisorbed and Chemisorbed Species, respectively.

	V_3C_2	Nb_3C_2	Cr_3C_2	Mo_3C_2
**CO ₂	-0.77	-0.67	-0.44	-1.01
**OCHO•	-1.32	-1.06	-1.12	-1.42
**•OCH ₂ O•	-1.38	-2.33	-0.83	-1.51
**HOCH ₂ O•	-1.41	-1.53	-0.94	-1.80
**H ₂ CO	-1.75	-1.84	-0.82	-1.74
**CH ₃ O•	-1.94	-2.47	-1.32	-2.18
**O ..*CH ₄	-1.99	-2.95	-1.23	-1.83
**OH•	-2.96	-3.30	-2.26	-3.08
**H ₂ O	-1.41	-1.55	-1.58	-1.84

Additionally, and as a paramount feature, DFT+*U*/DFT-D3 calculations of the d^3 V_3C_2 and Nb_3C_2 , and the d^4 Cr_3C_2 and Mo_3C_2 materials for the capture of H₂O, predict spontaneous Gibbs free binding energies, but always lower than the ones due to the CO₂ chemisorption (see **Fig. 2**). In other words, the selected materials are more selective to interact with CO₂ than with H₂O, offering promising perspectives for the use of these materials in a water environment.

Concerning the nature of the interactions when bonding CO₂ on the MXenes surfaces, the low-coordinated metals atoms are seen to interact through the C of CO₂, potentially *via* electron-donation from the carbides (proximal distances between 2.17 and 2.49 Å), and also synergistically supported through intense interactions between the O lone pairs from CO₂ to the aforementioned three-fold metal atoms (proximal distances between 1.92 and 2.34 Å). In the case of the chemisorbed H₂O molecules (**Fig. 2**), they bind through their O lone pairs to the metal atoms of the MXenes, showing also strong interactions, with ΔG_b between -0.21 and -0.64 eV. This is experimentally corroborated by the measured hydrophilic behavior of MXenes.²⁵

The role of selectivity is crucial and strongly depends on how the material catalyzes the successive elementary electro-reductions. In this regard, test calculations employing classical DFT including dispersion *via* the DFT-D2 method (see **Table 1**) predicts non-spontaneous Gibbs free reaction energies at room temperature (hereafter simply referred as reaction energies) for the first H⁺/e⁻ pair gain, that leads to the chemisorbed HOCO• and OCHO• radical species. However, the hydrogenation on the C atom of the captured CO₂ molecule is more thermodynamically preferred than when acting on one of the two terminal O atoms of CO₂. This implies that the competitive CO and HCOOH formation would be min-

imal compared to •OCH₂O• formation, which follows with the third H⁺/e⁻ transfer onto one of the still unreacted O atoms to obtain the HOCH₂O• intermediate species. As result of the fourth H⁺/e⁻ gain, H₂CO is produced (with the release of one H₂O molecule), notwithstanding it deserves to be mentioned that the release of this captured H₂CO requires the input of a large amount of energy as a consequence of the aforementioned strong interactions between substrate and surface.

With the exception of Hf₃C₂, the formation of CH₃O• as a fifth-reduced radical species, which is the precursor of CH₃OH, exhibits spontaneous reaction energies, however the sixth hydrogenation at the CH₃O• radical requires its release from the surface in order that the H⁺/e⁻ pair can physically access to it, leading to the appearance of energy limitations in the range of 3 eV or higher for d^2 and Ta₃C₂ MXenes, and around 2.5 eV for M₃C₂ when M = V, Nb, Cr, and Mo. This limiting step eliminates this path, as well as the path towards the formation of CH₄ that also requires the injection of an important amount of energy for the release of the seventh hydrogenated CH₃• radical. However, the reactive nature of the transition metal carbides establishes an alternative path, that like in the case of the theoretical model of highly-reactive beryllium-doped BNs,¹⁹ is thermodynamically preferred in the mechanism of CO₂ electro-reduction to CH₄. Such a mechanism involves the sixth H⁺/e⁻ pair gain on the CH₃O• radical taking place on the CH₃ moiety, leading first to the release of CH₄ and an O atom inserted on the material, and secondly, continuing with two successive hydrogenations that produce an -OH• doped solid and a captured H₂O molecule. Despite such H₂O product contaminating the material, relative small reaction energy (with respect the limiting **OH•/**H₂O step) is needed, and besides that potential new CO₂ molecules will thermodynamically displace the captured water.

Although our DFT predictions establish a common path being exhibited by all the M₃C₂ MXenes studied in the present work, it is clear that d^2 Ti₃C₂, Zr₃C₂, and Hf₃C₂, as well as d^3 Ta₃C₂, are not promising for the CO₂ conversion into hydrocarbon fuels due to the large limiting steps predicted. For this reason more accurate DFT+*U* calculations with explicit dispersion corrections *via* the DFT-D3 method have been carried out for the most promising d^3 V_3C_2 and Nb_3C_2 , and d^4 and Cr_3C_2 and Mo_3C_2 materials.

Thus, and as previously mentioned, the inclusion of the Hubbard-like parameters *via* the DFT+*U* approach to treat the strong on-site Coulomb interactions of the *d*-like localized electrons in M₃C₂ MXenes also predict spontaneous chemisorption processes of CO₂, however, values strongly differ due to the over-estimated interactions between CO₂ and the surface of the MXenes. Values of -0.77, -0.67, -0.44, and -1.01 eV are obtained for M = V, Nb, Cr, and Mo, respectively. Also, as a

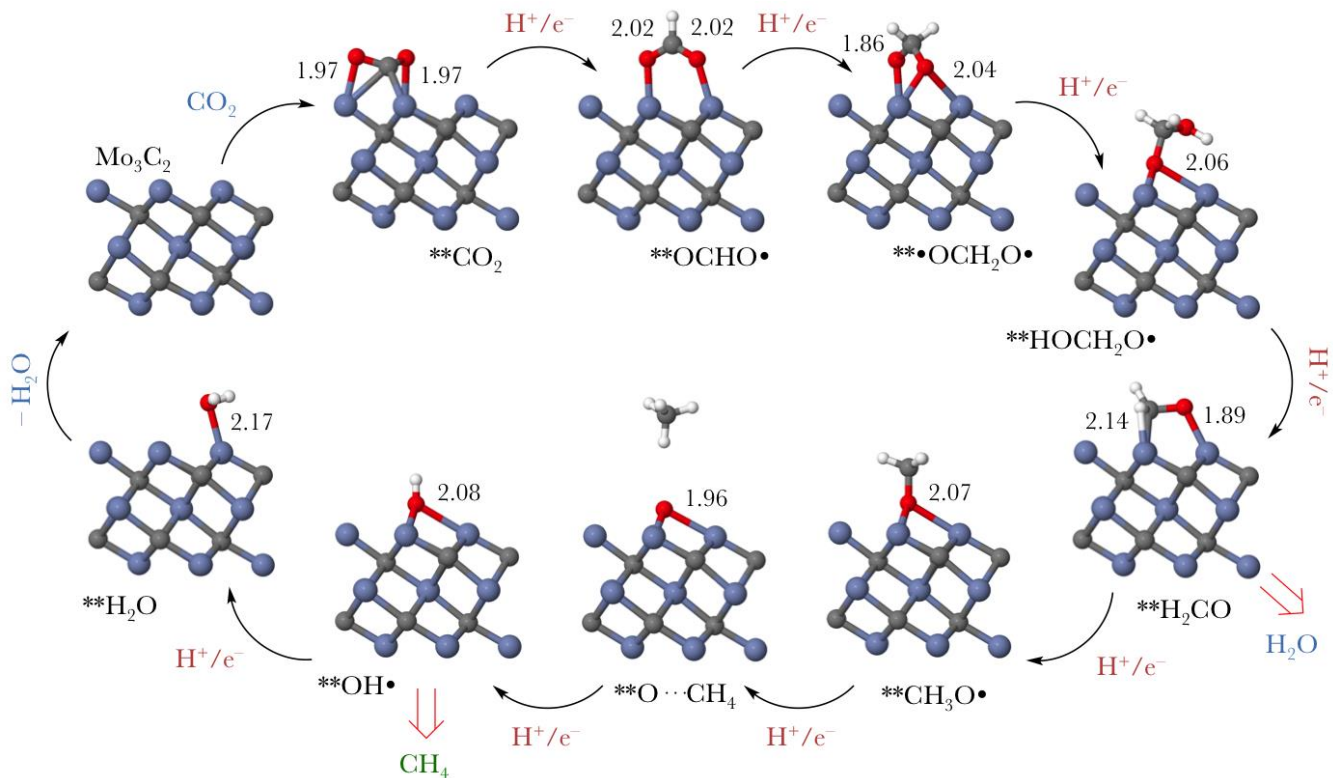


Figure 3. Minimum energy path (DFT+ U /DFT-D3 calculations, $U = 3.5$ eV) followed for the CO_2 conversion mechanism into *CH_4 and $\text{**H}_2\text{O}$ catalyzed by Cr_3C_2 . Note: Grey, lilac, red, and white spheres refer to C, Cr, O, and H atoms, in that order. Note: * and ** symbols refer to physisorbed and chemisorbed species, respectively. Selected distances are indicated in Å.

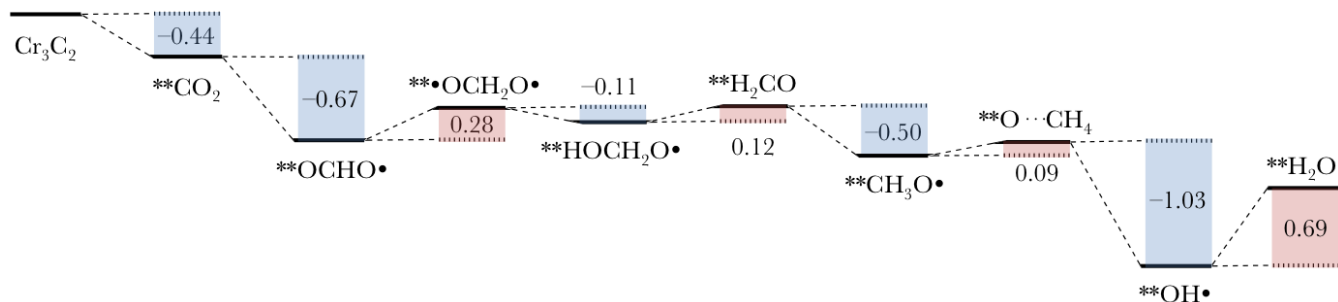


Figure 4. Gibbs free reaction energy diagram at 298.15 K (thermodynamics, in eV, referred to the immediately step) corresponding with the minimum energy path at the DFT+ U /DFT-D3 computational level for the CO_2 conversion mechanism into *CH_4 and $\text{**H}_2\text{O}$ catalyzed by Cr_3C_2 ($U = 3.5$ eV). Note: * and ** symbols refer to physisorbed and chemisorbed species, respectively.

common feature, spontaneous reaction energies are predicted for the first H^+/e^- gain to reach the $\text{OCHO}\bullet$ intermediate species, being -0.55 , -0.38 , -0.67 , and -0.41 eV, respectively. These results for this first electron-reduction process are of paramount importance, highlighting a novel and impressive outcome in the spontaneous production of the $\text{OCHO}\bullet$ radical, or in other words, overcoming the limitation imposed by this classically limiting step.¹⁸

With the exceptions of Nb_3C_2 and Cr_3C_2 , a cascade of spontaneous elementary reactions occur for the second and third hydrogenations to obtain the chemisorbed

$\bullet\text{OCH}_2\text{O}\bullet$ and $\text{HOCH}_2\text{O}\bullet$ intermediate species. Small reaction energy of 0.28 eV in the second H^+/e^- transfer is required for Cr_3C_2 , while $\text{HOCH}_2\text{O}\bullet$ demands 0.80 eV for Nb_3C_2 . Also, the d^3 MXenes show a different pattern in the production of H_2CO , which results in a highly distorted geometry with respect to the sp^2 hybridization as consequence of the strong interactions on the surface. This highlights the existence of a process that presents spontaneous reaction energies of -0.34 and -0.30 eV for $M = \text{V}$ and Nb , whereas for the d^4 series ($M = \text{Cr}$ and Mo) very low injections of energy, 0.12 and 0.06 eV, are needed. Furthermore, the $\text{CH}_3\text{O}\bullet$ is spontaneously pro-

duced in all these cases. However, it deserves to be mentioned that, with the exception of the 0.80 eV that Nb₃C₂ requires for the production of HOCH₂O•, the CO₂ conversion mechanism up to the fifth step follows a smooth path mainly characterized by spontaneous H⁺/e⁻ additions and their associated structural rearrangements.

As has been previously hypothesized, the CO₂ conversion mechanism catalyzed by *d*²-*d*⁴ M₃C₂ MXenes follows a common route in which the minimum energy path involves successive hydrogenations on the C and O atoms to reach OCHO•, •OCH₂O•, and HOCH₂O•, and obtaining H₂CO as fourth-order reduced species in the form of a highly distorted and captured product. Since the chemisorbed CH₃O• radical is more thermodynamically preferred than the chemisorbed H₂COH• one during the fifth H⁺/e⁻ pair gain, our DFT+*U*/DFT-D3 results also predict that the classical route towards the formation of the CH₃OH final product is not favored with respect to the sixth electro-reduction on the CH₃ moiety of the CH₃O• radical to reach a released CH₄ molecule and being an O atom covalently bounded on the material. As happened in the HOCH₂O• to H₂CO step, *d*³ MXenes are characterized to produce such ••O ··CH₄ in a spontaneous process, while for Cr₃C₂ and Mo₃C₂, the injection of 0.09 and 0.35 eV are required.

Finally, the O-doped moiety of the surface is presented as highly reactive, being proof of this the highly spontaneous reactions consisting in the seventh hydrogenation to reach the ••OH• radical species, that with exception of Nb₃C₂, indicates the maximum release of energy of all the elementary reactions (even more than the earlier CO₂ capture process). Unlike the classical materials in which the classical limiting step is imposed by the first hydrogenation step, our proposed materials present dramatically different behaviors, i.e. the release of such ••OH• radical species in the form of a relatively intense chemisorbed H₂O molecule once the eighth and final H⁺/e⁻ transfer comes into play. In this regard, *d*³ MXenes exhibit values of 1.55, 1.75, and 1.24 eV for M = V, Nb, and Mo, which are relatively high with respect to the impressive catalytic performance shown by Cr₃C₂, which, as shown in **Figs. 3** and **4**, is hypothesized as the best alternative for the catalytic reduction of CO₂ based on transition metal carbide catalysis at the present time. For comparative purposes, the limiting step of the Cr₃C₂ outcomes are in the other of some tested and/or theoretically studied materials as for instance: Cu surface (Peterson *et al.*, CO₂ to CH₄, limiting step of 740 mV),²⁰ or graphene-supported amorphous MoS₂ (Li *et al.*, CO₂ to CO, over-potential of 540 mV when acting at a maximum faradaic efficiency).⁶⁴

SUMMARY AND CONCLUSIONS

In summary, our theoretical calculations predict that 2D *d*², *d*³, and *d*⁴ transition metal carbides (MXenes) with formulae M_{*n*+1}C_{*n*} (*n* = 2) are capable of catalyzing CO₂

conversion into hydrocarbon compounds, being selective towards the formation of CH₄. Attending to the reaction energies computed in the present work by DFT modeling, *d*³ V₃C₂ and Nb₃C₂, and *d*⁴ and Cr₃C₂ and Mo₃C₂ materials offer the most promising results with limiting Gibbs free reaction energies at 298.15 K of 1.55, 1.75, 0.69, and 1.24 eV, respectively, according to the outcomes obtained at DFT+*U* computational level plus explicit DFT-D3 dispersion corrections. Although the highly reactive behaviors of these set of Group IVB carbides (in addition to *d*³ Ta₃C₂), the selected MXenes demonstrate active behaviors for the capture of CO₂, specially for those from the *d*² series (M = Ti, Zr, and Hf), dismissing their applicability in the conversion process. An analysis in-depth of the CO₂ conversion mechanism indicates that the minimum energy path follows an alternative route leading to the release of CH₄ during the sixth step, prior to the final H₂O production. Important features have been predicted during the first hydrogenation step towards the formation of the OCHO• radical species, offering spontaneous energies for the promising MXenes. This point is of considerable significance since the first electro-reduction classically creates the severest obstacle of the entire reaction. Moreover, it is hypothesized that the capture of CO₂ during the early step of the process is spontaneous without passing through a physisorbed state. The strength of such capture is even larger than the computed binding energies for the chemisorption of H₂O. Against this background, we provide novel insights into the computer-aided catalyst design and the reaction mechanism modeling of the CO₂ conversion catalysts. We offer encouraging perspectives for the experimental testing of these materials in a water environment, profiling Cr₃C₂ as the best alternative of these series of MXenes with a limiting reaction energy of 0.69 eV.

ASSOCIATED CONTENT

Supporting Information. Supporting Information contains: additional computational details, Gibbs free energies, density of states (HSE06 functional),⁶⁵⁻⁶⁶ and Cartesian coordinates allowing an unambiguous reproducibility of the theoretical outcomes discussed in the present work. This material is available free of charge *via* the Internet at <http://pubs.acs.org>.

AUTHORS INFORMATION

Corresponding Authors

*CS. Tel: (+61) 3 9902 9916. Fax: (+61) 3 9905 4597. E-mail: Chenghua.Sun@monash.edu

Author Contributions

All authors have given approval to the final version of the manuscript. [‡]NL and LMA have equally contributed to the development of this work.

Notes

Authors declare no competing financial interests.

ACKNOWLEDGMENTS

NL acknowledges the National Natural Science Foundation of China (Grant Nos. 51461135004, 51402225), the Doctoral Fund of Ministry of Education Priority Development Projects (Nos. 20130143130002, 20150303001), the Natural Science Foundation (NSF) of Hubei Province (No. 2015CFB227), the Key Technology Innovation Project of Hubei Province (No. 2013AAA005), the Fundamental Research Funds for the Central Universities (WUT: 2015-IVA-051), and the research board of the State Key Laboratory of Silicate Materials for Architectures (No. 47152005). LMA, DRM, and CS acknowledge the Australian Research Council (ARC) for its support through the ARC Centre of Electromaterials Science (ACES), Discover Project (DP130100268, CS), Future Fellowship (FT130100076, CS), and Laureate Fellow (DRM) schemes. We also thank the National Energy Research Scientific Computing Center in Shanghai and the National Computational Infrastructure (NCI), which is supported by the Australian Government, for providing the computational resources.

REFERENCES

- (1) Maginn, E. J. What to Do with CO₂. *J. Phys. Chem. Lett.* **2010**, *1*, 3478-3479.
- (2) Karl, T. R.; Trenberth, K. E. Modern Global Climate Change. *Science* **2003**, *302*, 1719-1723.
- (3) Kondratenko, E. V.; Mul, G.; Baltrusaitis, J.; Larrazabal, G. O.; Pérez-Ramírez, J. Status and Perspectives of CO₂ Conversion into Fuels and Chemicals by Catalytic, Photocatalytic and Electrocatalytic Processes. *Energy Environ. Sci.* **2013**, *6*, 3112-3135.
- (4) Varghese, O. K.; Paulose, M.; LaTempa, T. J.; Grimes, C. A. High-Rate Solar Photocatalytic Conversion of CO₂ and Water Vapor to Hydrocarbon Fuels. *Nano Lett.* **2009**, *9*, 731-737.
- (5) Liu, G.; Hoiwik, N.; Wang, K.; Jakobsen, H. Engineering TiO₂ Nanomaterials for CO₂ Conversion/Solar Fuels. *Sol. Energy Mater. Sol. Cells* **2012**, *105*, 53-68.
- (6) Zhao, C.; Liu, L.; Zhang, Q.; Wang, J.; Li, Y. Photocatalytic Conversion of CO₂ and H₂O to Fuels by Nanostructured Ce-TiO₂/SBA-15 Composites. *Catal. Sci. Tech.* **2012**, *2*, 2558-2568.
- (7) Graciani, J.; Mudiyanse, K.; Xu, F.; Baber, A. E.; Evans, J.; Senanayake, S. D.; Stacchiola, D. J.; Liu, P.; Hrbek, J.; Sanz, J. F.; Rodriguez, J. A. Highly Active Copper-Ceria and Copper-Ceria-Titania Catalysts for Methanol Synthesis from CO₂. *Science* **2014**, *345*, 546-550.
- (8) Lim, D.-H.; Jo, J. H.; Shin, D. Y.; Wilcox, J.; Ham, H. C.; Nam, S. W. Carbon Dioxide Conversion into Hydrocarbon Fuels on Defective Graphene-Supported Cu Nanoparticles from First Principles. *Nanoscale* **2014**, *6*, 5087-5092.
- (9) Li, H.; Zhang, X.; MacFarlane, D. R. Carbon Quantum Dots/Cu₂O Heterostructures for Solar-Light-Driven Conversion of CO₂ to Methanol. *Adv. Energy Mater.* **2015**, *5*, 1401077.
- (10) Hsu, H.-C.; Shown, I.; Wei, H.-Y.; Chang, Y.-C.; Du, H.-Y.; Lin, Y.-G.; Tseng, C.-A.; Wang, C.-H.; Chen, L.-C.; Lin, Y.-C.; Chen, K.-H. Graphene Oxide as a Promising Photocatalyst for CO₂ to Methanol Conversion. *Nanoscale* **2013**, *5*, 262-268.
- (11) Mao, J.; Peng, T.; Zhang, X.; Li, K.; Ye, L.; Zan, L. Effect of Graphitic Carbon Nitride Microstructures on the Activity and Selectivity of Photocatalytic CO₂ Reduction under Visible Light. *Catal. Sci. Tech.* **2013**, *3*, 1253-1260.
- (12) Rosen, B. A.; Salehi-Khojin, A.; Thorson, M. R.; Zhu, W.; Whipple, D. T.; Kenis, P. J. A.; Masel, R. I. Ionic Liquid-Mediated Selective Conversion of CO₂ to CO at Low Overpotentials. *Science* **2011**, *334*, 643-644.
- (13) DiMaggio, J. L.; Rosenthal, J. Selective Conversion of CO₂ to CO with High Efficiency Using an Inexpensive Bismuth-Based Electrocatalyst. *J. Am. Chem. Soc.* **2013**, *135*, 8798-8801.
- (14) Li, P.; Jing, H.; Xu, J.; Wu, C.; Peng, H.; Lu, J.; Lu, F. High-Efficiency Synergistic Conversion of CO₂ to Methanol using Fe₂O₃ Nanotubes Modified with Double-Layer Cu₂O Spheres. *Nanoscale* **2014**, *6*, 11380-11386.
- (15) He, Y.; Wang, Y.; Zhang, L.; Teng, B.; Fan, M. High-Efficiency Conversion of CO₂ to Fuel over ZnO/g-C₃N₄ Photocatalyst. *Appl. Catal. B Environ.* **2015**, *168-169*, 1-8.
- (16) Whipple, D. T.; Kenis, P. J. A. Prospects of CO₂ Utilization via Direct Heterogeneous Electrochemical Reduction. *J. Phys. Chem. Lett.* **2010**, *1*, 3451-3458.
- (17) Habisreutinger, S. N.; Schmidt-Mende, L.; Stolarczyk, J. K. Photocatalytic Reduction of CO₂ on TiO₂ and Other Semiconductors. *Angew. Chem. Int. Ed.* **2013**, *52*, 7372-7408.
- (18) Koppenol, W. H.; Rush, J. D. Reduction Potential of the Carbon Dioxide/Carbon Dioxide Radical Anion: A Comparison with other C1 Radicals. *J. Phys. Chem.* **1987**, *91*, 4429-4430.
- (19) Azofra, L. M.; MacFarlane, D. R.; Sun, C. And Intensified π -Hole in Beryllium-Doped Boron Nitride Meshes: Its Determinant Role in the CO₂ Conversion into Hydrocarbon Fuels. *Chem. Commun.* **2016**, *52*, 3548-3551.
- (20) Peterson, A. A.; Abild-Pedersen, F.; Studt, F.; Rossmeisl, J.; Nørskov, J. K. How Copper Catalyzes the Electroreduction of Carbon Dioxide into Hydrocarbon Fuels. *Energy Environ. Sci.* **2010**, *3*, 1311-1315.
- (21) Peterson, A. A.; Nørskov, J. K. Activity Descriptors for CO₂ Electroreduction to Methane on Transition-Metal Catalysts. *J. Phys. Chem. Lett.* **2012**, *3*, 251-258.
- (22) Lang, L. Beryllium: A Chronic Problem. *Environ. Health Perspect.* **1994**, *102*, 526-531.
- (23) Naguib, M.; Kurtoglu, M.; Presser, V.; Lu, J.; Niu, J.; Heon, M.; Hultman, L.; Gogotsi, Y.; Barsoum, M. W. Two-Dimensional Nanocrystals Produced by Exfoliation of Ti₃AlC₂. *Adv. Mater.* **2011**, *23*, 4248-4253.
- (24) Naguib, M.; Mochalin, V. N.; Barsoum, M. W.; Gogotsi, Y. 25th Anniversary Article: MXenes: A New Family of Two-Dimensional Materials. *Adv. Mater.* **2014**, *26*, 992-1005.
- (25) Naguib, M.; Mashtalir, O.; Carle, J.; Presser, V.; Lu, J.; Hultman, L.; Gogotsi, Y.; Barsoum, M. W. Two-Dimensional Transition Metal Carbides. *ACS Nano* **2012**, *6*, 1322-1331.
- (26) Naguib, M.; Halim, J.; Lu, J.; Cook, K. M.; Hultman, L.; Gogotsi, Y.; Barsoum, M. W. Two-Dimensional Niobium and Vanadium Carbides as Promising Materials for Li-Ion Batteries. *J. Am. Chem. Soc.* **2013**, *135*, 15966-15969.
- (27) Yang, J.; Naguib, M.; Ghidui, M.; Pan, L.-M.; Gu, J.; Nanda, J.; Halim, J.; Gogotsi, Y.; Barsoum, M. W. Two-Dimensional Nb-Based M₄C₃ Solid Solutions (MXenes). *J. Am. Ceram. Soc.* **2015**, *in press*. DOI: 10.1111/jace.13922
- (28) Anasori, B.; Xie, Y.; Beidaghi, M.; Lu, J.; Hosler, B. C.; Hultman, L.; Kent, P. R. C.; Gogotsi, Y.; Barsoum, M. W. Two-Dimensional, Ordered, Double Transition Metals Carbides (MXenes). *ACS Nano* **2015**, *9*, 9507-9516.
- (29) Naguib, M.; Come, J.; Dyatkin, B.; Presser, V.; Taberna, P.-L.; Simon, P.; Barsoum, M. W.; Gogotsi, Y. MXene: A Promising Transition Metal Carbide Anode for Lithium-Ion Batteries. *Electrochem. Commun.* **2012**, *16*, 61-64.
- (30) Xie, Y.; Naguib, M.; Mochalin, V. N.; Barsoum, M. W.; Gogotsi, Y.; Yu, X.; Nam, K.-W.; Yang, X.-Q.; Kolesnikov, A. I.; Kent, P. R. C. Role of Surface Structure on Li-Ion Energy Storage Capacity of Two-Dimensional Transition-Metal Carbides. *J. Am. Chem. Soc.* **2014**, *136*, 6385-6394.
- (31) Liang, X.; Garsuch, A.; Nazar, L. F. Sulfur Cathodes Based on Conductive MXene Nanosheets for High-Performance Lithium-Sulfur Batteries. *Angew. Chem. Int. Ed.* **2015**, *54*, 3907-3911.
- (32) Er, D.; Li, J.; Naguib, M.; Gogotsi, Y.; Shenoy, V. B. Ti₃C₂ MXene as a High Capacity Electrode Material for Metal (Li, Na, K, Ca) Ion Batteries. *ACS Appl. Mater. Interfaces* **2014**, *6*, 11173-11179.
- (33) Lukatskaya, M. R.; Mashtalir, O.; Ren, C. E.; Dall'Agnese, Y.; Rozier, P.; Taberna, P. L.; Naguib, M.; Simon, P.; Barsoum, M. W.; Gogotsi, Y. Cation Intercalation and High Volumetric Capacitance of Two-Dimensional Titanium Carbide. *Science* **2013**, *341*, 1502-1505.
- (34) Ghidui, M.; Lukatskaya, M. R.; Zhao, M.-Q.; Gogotsi, Y.; Barsoum, M. W. Conductive Two-Dimensional Titanium Carbide 'Clay' with High Volumetric Capacitance. *Nature* **2014**, *516*, 78-81.
- (35) Wang, X.; Kajiyama, S.; Iinuma, H.; Hosono, E.; Oro, S.; Moriguchi, I.; Okubo, M.; Yamada, A. Pseudocapacitance of MXene

- Nanosheets for High-Power Sodium-Ion Hybrid Capacitors. *Nat. Commun.* **2015**, *6*, 6544.
- (36) Xie, X.; Chen, S.; Ding, W.; Nie, Y.; Wei, Z. An Extraordinarily Stable Catalyst: Pt NPs supported on Two-Dimensional $Ti_3C_2X_2$ ($X = OH, F$) Nanosheets for Oxygen Reduction Reaction. *Chem. Commun.* **2013**, *49*, 10112-10114.
- (37) Mashtalir, O.; Cook, K. M.; Mochalin, V. N.; Crowe, M.; Barsoum, M. W.; Gogotsi, Y. Dye Adsorption and Decomposition on Two-Dimensional Titanium Carbide in Aqueous Media. *J. Mater. Chem. A* **2014**, *2*, 14334-14338.
- (38) Chen, W.-F.; Muckerman, J. T.; Fujita, E. Recent Developments in Transition Metal Carbides and Nitrides as Hydrogen Evolution Electrocatalysts. *Chem. Commun.* **2013**, *49*, 8896-8909.
- (39) Liu, H.; Duan, C.; Yang, C.; Shen, W.; Wang, F.; Zhu, Z. A Novel Nitrite Biosensor based on the Direct Electrochemistry of Hemoglobin Immobilized on MXene- Ti_3C_2 . *Sens. Actuators, B* **2015**, *218*, 60-66.
- (40) Halim, J.; Lukatskaya, M. R.; Cook, K. M.; Lu, J.; Smith, C. R.; Nöslund, L.-Å.; May, S. J.; Hultman, L.; Gogotsi, Y.; Eklund, P.; Barsoum, M. W. Transparent Conductive Two-Dimensional Titanium Carbide Epitaxial Thin Films. *Chem. Mater.* **2014**, *26*, 2374-2381.
- (41) Furimsky, E. Metal Carbides and Nitrides as Potential Catalysts for Hydroprocessing. *Appl. Catal., A* **2003**, *240*, 1-28.
- (42) Peng, Q.; Guo, J.; Zhang, Q.; Xiang, J.; Liu, B.; Zhou, A.; Liu, R.; Tian, Y. Unique Lead Adsorption Behavior of Activated Hydroxyl Group in Two-Dimensional Titanium Carbide. *J. Am. Chem. Soc.* **2014**, *136*, 4113-4116.
- (43) Liu, Y.; Kelly, T. G.; Chen, J. G.; Mustain, W. E. Metal Carbides as Alternative Electrocatalyst Supports. *ACS Catal.* **2013**, *3*, 1184-1194.
- (44) Chen, W. F.; Wang, C. H.; Sasaki, K.; Marinkovic, N.; Xu, W.; Muckerman, J. T.; Zhu, Y.; Adzic, R. R. Highly Active and Durable Nanostructured Molybdenum Carbide Electrocatalysts for Hydrogen Production. *Energy Environ. Sci.* **2013**, *6*, 943-951.
- (45) Lee, J. S. Metal Carbides, *Encyclopedia of Catalysis*, John Wiley & Sons, Inc., 2002.
- (46) Perdew, J. P.; Burke, K.; Ernzerhof, M. Generalized Gradient Approximation Made Simple. *Phys. Rev. Lett.* **1996**, *77*, 3865-3868.
- (47) Blöchl, P. E. Projector Augmented-Wave Method. *Phys. Rev. B* **1994**, *50*, 17953-17979.
- (48) Kresse, G.; Joubert, D. From Ultrasoft Pseudopotentials to the Projector Augmented-Wave Method. *Phys. Rev. B* **1999**, *59*, 1758-1775.
- (49) Grimme, S. Semiempirical GGA-Type Density Functional Constructed with a Long-Range Dispersion Correction. *J. Comput. Chem.* **2006**, *27*, 1787-1799.
- (50) Liechtenstein, A. I.; Anisimov, V. I.; Zaanen, J. Density-Functional Theory and Strong Interactions: Orbital Ordering in Mott-Hubbard Insulators. *Phys. Rev. B* **1995**, *52*, R5467-R5470.
- (51) Dudarev, S. L.; Botton, G. A.; Savrasov, S. Y.; Humphreys, C. J.; Sutton, A. P. Electron-Energy-Loss Spectra and the Structural Stability of Nickel Oxide: An LSDA+ U Study. *Phys. Rev. B* **1998**, *57*, 1505-1509.
- (52) Finazzi, E.; Di Valentin, C.; Pacchioni, G.; Selloni, A. Excess Electron States in Reduced Bulk Anatase TiO_2 : Comparison of Standard GGA, GGA+ U , and Hybrid DFT Calculations. *J. Chem. Phys.* **2008**, *129*, 154113.
- (53) Jain, A.; Hautier, G.; Ong, S. P.; Moore, C. J.; Fischer, C. C.; Persson, K. A.; Ceder, G. Formation Enthalpies by Mixing GGA and GGA+ U Calculations. *Phys. Rev. B* **2011**, *84*, 045115.
- (54) Stevanović, V.; Lany, S.; Zhang, X.; Zunger, A. Correcting Density Functional Theory for Accurate Predictions of Compound Enthalpies of Formation: Fitted Elemental-Phase Reference Energies. *Phys. Rev. B* **2012**, *85*, 115104.
- (55) Sun, C.; Liao, T.; Lu, G. Q.; Smith, S. C. The Role of Atomic Vacancy on Water Dissociation over Titanium Dioxide Nanosheet: A Density Functional Theory Study. *J. Phys. Chem. C* **2012**, *116*, 2477-2482.
- (56) Grimme, S.; Antony, J.; Ehrlich, S.; Krieg, H. A Consistent and Accurate *Ab Initio* Parametrization of Density Functional Dispersion Correction (DFT-D) for the 94 Elements H-Pu. *J. Chem. Phys.* **2010**, *132*, 154104.
- (57) Grimme, S.; Ehrlich, S.; Goerigk, L. Effect of the Damping Function in Dispersion Corrected Density Functional Theory. *J. Comput. Chem.* **2011**, *32*, 1456-1465.
- (58) Kresse, G.; Hafner, J. *Ab Initio* Molecular Dynamics for Liquid Metals. *Phys. Rev. B* **1993**, *47*, 558-561.
- (59) Kresse, G.; Hafner, J. *Ab Initio* Molecular-Dynamics Simulation of the Liquid-Metal-Amorphous-Semiconductor Transition in Germanium. *Phys. Rev. B* **1994**, *49*, 14251-14269.
- (60) Kresse, G.; Furthmüller, J. Efficient Iterative Schemes for *Ab Initio* Total-Energy Calculations using a Plane-Wave Basis Set. *Phys. Rev. B* **1996**, *54*, 11169-11186.
- (61) Kresse, G.; Furthmüller, J. Efficiency of *Ab-Initio* Total Energy Calculations for Metals and Semiconductors using a Plane-Wave Basis Set. *Comput. Mat. Sci.* **1996**, *6*, 15-50.
- (62) Yin, W.-J.; Krack, M.; Wen, B.; Ma, S.-Y.; Liu, L.-M. CO_2 Capture and Conversion on Rutile $TiO_2(110)$ in the Water Environment: Insight by First-Principles Calculations. *J. Phys. Chem. Lett.* **2015**, *6*, 2538-2545.
- (63) While preparing this manuscript, a similar research concerning the function of transition metal carbides as CO_2 capture materials has appeared at: Kunkel, C.; Viñes, F.; Illas, F. Transition Metal Carbides as Novel Materials for CO_2 Capture, Storage, and Activation. *Energy Environ. Sci.*, **2016**, *9*, 141-144.
- (64) Li, F.; Zhao, S.-F.; Chen, L.; Khan, A.; MacFarlane, D. R.; Zhang, J. Polyethylenimine Promoted Electrocatalytic Reduction of CO_2 to CO in Aqueous Medium by Graphene-Supported Amorphous Molybdenum Sulphide. *Energy Environ. Sci.* **2016**, *9*, 216-223.
- (65) Heyd, J.; Scuseria, G. E.; Ernzerhof, M. Hybrid Functionals based on a Screened Coulomb Potential. *J. Chem. Phys.* **2003**, *118*, 8207-8215. See *Erratum* at: Heyd, J.; Scuseria, G. E.; Ernzerhof, M. Hybrid Functionals based on a Screened Coulomb Potential. *J. Chem. Phys.* **2006**, *124*, 219906.
- (66) Heyd, J.; Scuseria, G. E. Efficient Hybrid Density Functional Calculations in Solids: Assessment of the Heyd-Scuseria-Ernzerhof Screened Coulomb Hybrid Functional. *J. Chem. Phys.* **2004**, *121*, 1187-1192.

